Volume 1 | Number 1 | Jan 2013 | Pages 1–100

Nanoscale

www.rsc.org/nanoscale

ROYAL SOCIETY OF CHEMISTRY

ROYAL SOCIETY OF CHEMISTRY

www.rsc.org/nanoscale

Nanoscale

PAPER

High second-order nonlinear response of platinum nanoflowers: the role of surface corrugation†

Hoang Minh Ngo, Ngoc Diep Lai and Isabelle Ledoux-Rak[*]

Platinum nanoflowers (PtNFs) were elaborated using the seed-mediated growth technique applied to monodisperse platinum nanoparticles (~3.0 nm) synthesized by the chemical reduction method. The X-ray diffraction pattern confirmed the formation of face-centered-cubic platinum nanocrystals. We report the Harmonic Light Scattering (HLS) properties of PtNFs for six different diameters (~7.0; 8.0; 10.0; 14.0; 20.0 and 31.0 nm). From these HLS data we infer, for the first time, large hyperpolarizability β values of PtNFs. These very high β values of PtNFs are assigned mainly to highly corrugated surfaces for nanoparticles with irregular shapes.

Introduction

Noble metal nanoparticles made of gold, silver and platinum exhibit unique optical properties related to surface plasmon resonance (SPR) effects at nanoscale, strongly differing from their corresponding bulk metals, and have been therefore the focus of many investigations for potential applications in optoelectronic and biophotonic devices.[1–8] The quadratic nonlinear optical properties of metallic nanoparticles are usually defined by their hyperpolarizability β values. The second harmonic generation (SHG) technique named Harmonic Light Scattering (HLS)[9,10] is used for the determination of the first hyperpolarizability tensor β, both for molecules and nanoparticles. Their β value depends on their size, shape, material and crystal structure, etc. Among them, exceptionally strong hyperpolarizability tensors of gold and silver nanoparticles have been reported[11–24] with potential promising applications, for example as biosensors.

Platinum nanoparticle-(PtNPs)-based catalysts are vital to fuel cells, sensors, petroleum and automotive industries, and to optoelectronic and biophotonic devices, due to their high catalytic activity and stability.[25–42] As for other metallic nano-objects, their optical properties exhibit a strong dependence on the nanoparticle morphology. Many investigations have been focused on controlling the shape and size of PtNPs.[43–52] Up to now, no significant β values of PtNPs have been reported yet. The plasmon resonance of Pt being located in the UV range ($\lambda \leq 200$ nm), authors did not evidence significant β values in PtNPs during their investigations by HLS measurements of various metallic NPs.[23]

In this paper, we report, for the first time, the evidence of a strong quadratic nonlinear response for platinum nanoflowers (PtNFs). These nanoflowers were synthesized in aqueous solution by the chemical reduction[53,54] and seed-mediated methods.[52,55–57] The resulting nanoflowers were characterized by UV–Vis absorption spectroscopy, X-ray diffraction (XRD), transmission electron microscopy (TEM) and SHG.

Results and Discussion

The nanoflowers synthesis reactions are very fast in mild heating (100 ^{0}C) conditions in the presence of a strong reducing agent such as ascorbic acid. The H_2PtCl_6 aqueous solution is pale yellow and shows a peak at 259 nm in its UV-Vis spectrum as shown in Fig. 1. On the other hand, H_2PtCl_6 in tri-sodium citrate (TSC) solution shows the same peak at 259 nm, characteristic of the $[PtCl_6]^{2-}$ complex. The color of the solution becomes brown yellow and finally becomes pale brown when adding ascorbic acid. This pale brown color at a 1.92×10^{-4} M concentration is due to the very broad absorption band related to the Pt plasmonic resonance, this band extending far away from its maximum within the visible range (see insert in Fig. 1). The $[PtCl_6]^{2-}$ peak at 259 nm in the UV-Vis spectrum disappears, suggesting that most of $[PtCl_6]^{2-}$ ions are reduced, so the reaction process is almost complete.[49,58]

Laboratoire de Photonique Quantique et Moléculaire, UMR 8537, Ecole Normale Supérieure de Cachan, CentraleSupélec, CNRS, Université Paris-Saclay, 94235 Cachan, France. E-mail: ledoux@lpqm.ens-cachan.fr

†Electronic Supplementary Information (ESI) available: The recalculated β and β' values inferred from data by Galletto et al.[15] in AuNSs using their reported β values per nanoparticle corrected. See DOI: 10.1039/x0xx00000x

Nanoscale Accepted Manuscript
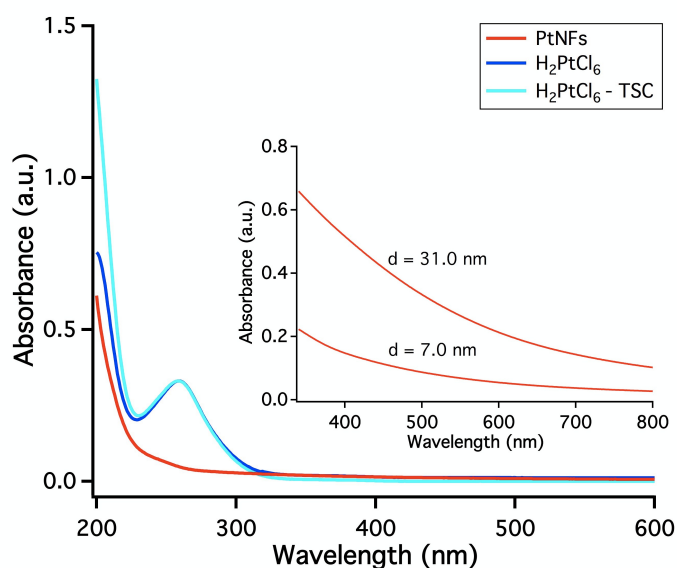
Fig. 1 UV-Visible-absorption spectra of the PtNFs solution, H_2PtCl_6 and H_2PtCl_6-TSC, C_{Pt} = 1.6 × 10^{-5} M. Insert: Visible absorption spectra of two solutions of PtNFs of different diameters, C_{Pt} = 1.92 × 10^{-4} M.

The XRD of PtNFs obtained by reduction by ascorbic acid exhibits diffraction peaks at 2θ between 40 and 85° as shown in Fig. 2. These XRD data confirmed the formation of face-centered-cubic (fcc, a = 3.92 Å) Pt nanocrystals at 2θ values of 40^0; $46,5^0$, 68^0 and 81^0 representing the (111), (200), (220) and (311) planes of the fcc structure.
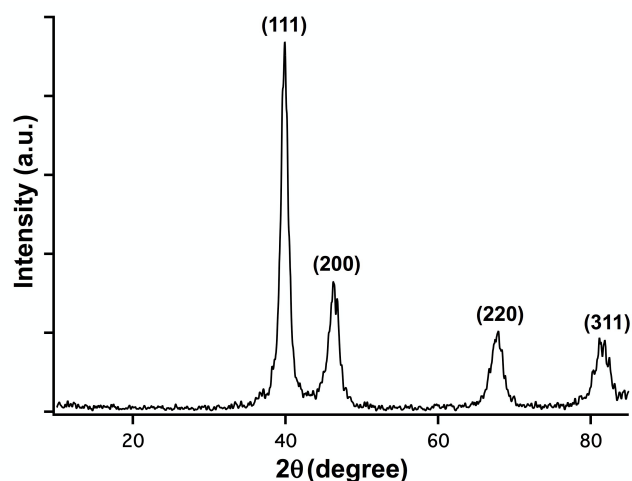
Fig. 2 XRD pattern of the PtNFs.

The size and shape of particles were determined with TEM imaging. Samples for TEM were prepared by dropping a platinum colloidal solution onto a carbon-coated Cu grid, followed by slow evaporation of solvent at room temperature. Fig. 3 shows TEM images of PtNFs and indicates the average diameter of the particles obtained by measuring and averaging diameters for about 100 particles. Higher resolution insets clearly confirm that most of PtNP's are "nanoflowers".
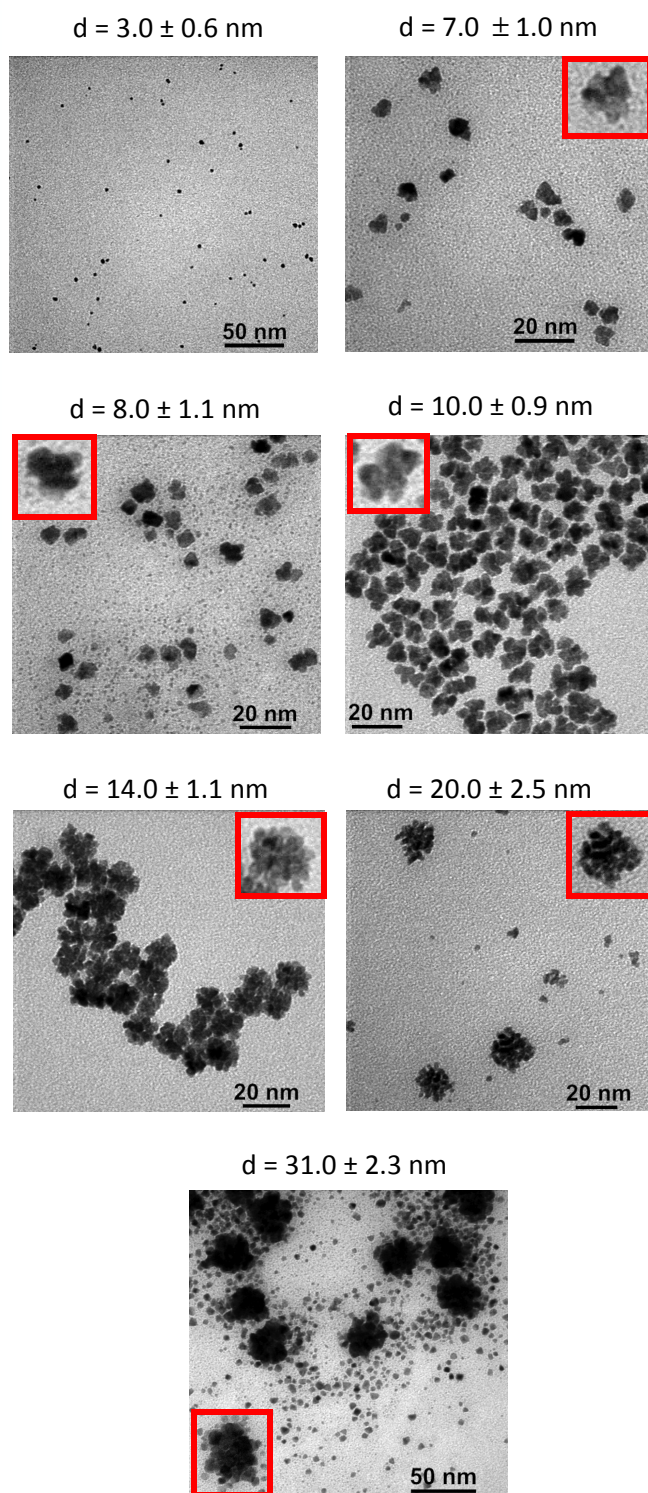
Fig. 3 TEM images of PtNFs with various sizes. The diameter d of nanoflowers is determined by averaging diameter values of 100 particles.

Freshly prepared solutions of PtNFs were characterized by HLS at 1.064 μm for the determination of their first order hyperpolarizability, on the basis of a known β value of the water solvent used as a reference. This β value of water is first measured by HLS using chloroform as a reference (β_{CHCl3} = 0.19 ± 0.02 × 10^{-30} esu at 1.06 μm). We then inferred a β value for water β_{H2O} = 0.055 × 10^{-30} esu.[11] We have checked that the HLS signal arises only from a SHG process and not from broadband visible emission from laser-induced damage on PtNFs (see below). As the plasmonic resonance wavelength is very far away from fundamental and harmonic laser wavelengths, no fluorescence signal (one- or two-photons) is observed for PtNFs.

The β per particle is calculated by using the equation below:

$$\frac{P}{P_0} = \frac{\left[N_{NPs}\left\langle\beta_{NPs}^2\right\rangle + N_{H_2O}\left\langle\beta_{H_2O}^2\right\rangle \right]}{N_{H_2O}\left\langle\beta_{H_2O}^2\right\rangle} \qquad (1)$$

where N_{NPs}, β_{NPs} and P are respectively the concentration of the nanoparticles, the first hyperpolarizability and the slope of the HLS intensity of nanoparticle recorded from solutions, N_{H2O}, β_{H2O} and P_0 are respectively the concentration of water, the first hyperpolarizability and the slope of the HLS intensity recorded from pure water. The concentration of the particles is calculated from the known concentration of the initial platinum solution, and from the average volume of nanoparticles.

Fig. 4 shows the SH intensity observed for pure water and for a PtNFs solution plotted with respect to the SH intensity collected from a NPP (N-4-nitrophenyl-prolinol)[59] powder (frequency doubler) at a 1064 nm fundamental wavelength.[11] The linear variation of this HLS signal with respect to $I_{NNP}^{2\omega}$ precludes any contribution from laser-induced damage on PtNFs, this latter phenomenon being characterized by a clear depart from this expected linear behavior beyond a given $I_{NNP}^{2\omega}$ value (threshold phenomenon). The value of the slope P displays a linear dependence with nanoparticle concentration (Fig. 5), as expected from Eq. 1.
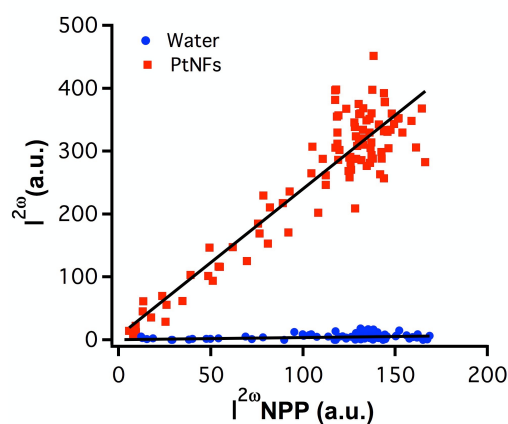
Fig. 4 Comparison between the SH intensity recorded from pure water (blue disks) and from 3.5 × 10^{-10} M PtNFs solution (red squares) with respect to the SH intensity collected from the NPP powder at 1064 nm fundamental wavelength.
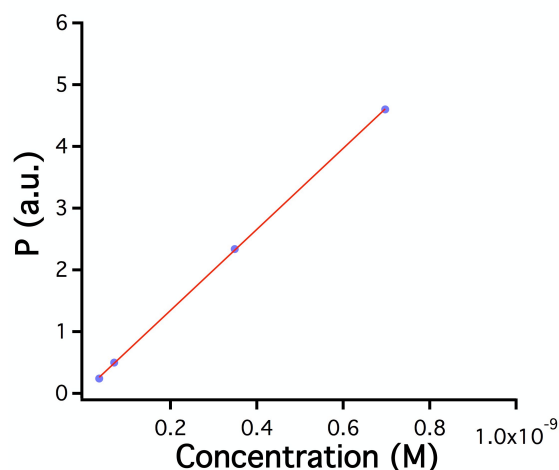
Fig. 5 The slope of the HLS intensity of nanoparticle recorded from PtNFs solutions (20nm) with different nanoparticle concentrations. The straight lines results from a linear fit with a remarkable correlation coefficient (0.999).

Table 1 First hyperpolarizability (β) values of Pt per atom and per particle. The relative experimental error on β is ± 15%, mainly due to the uncertainly from HLS measurements in water, the signal/noise ratio for the SHG signal being much lower in this case than for PtNFs solutions.

Sample	Diameter (nm)	Volume (nm^3)	N_{Pt} per particle (× 10^3)	Particle concentration	β per particle (β) (× 10^{-26} esu)	β per Pt atom (β') (× 10^{-30} esu)	Surface area (nm^2)
PtNF 1	7.0	180	12	1.63E-08	2.8	260	150
PtNF 2	8.0	270	18	1.09E-08	3.8	280	200
PtNF 3	10.0	520	34	5.60E-09	5.7	310	310
PtNF 4	14.0	1400	95	2.04E-09	11.3	370	620
PtNF 5	20.0	4200	280	3.48E-10	23.5	450	1300
PtNF 6	31.0	15600	1026	3.12E-11	61.0	600	3000

Remarkably high β values of PtNFs are measured and presented in Table 1. When comparing β values of PtNFs to the results of gold nanospheres (AuNSs) obtained by Galletto et al.,[15] for particles with the same diameter range (4.9-22 nm), our results for PtNFs (from 2.8 to 23.5×10^{-26} esu) are higher than the values of AuNSs obtained in the literature (from 0.6 to 16.6×10^{-26} esu).

(a)

(b)
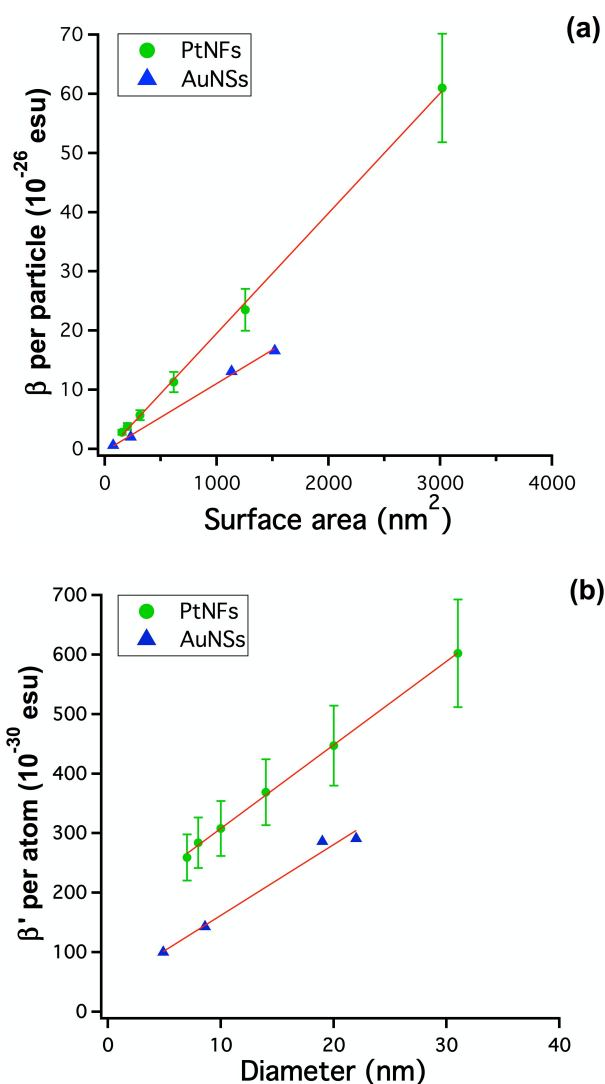
Fig. 6 (a) HLS values of the first hyperpolarizability (β) per Pt particle (green disks, this work) and per Au particle[15] (blue triangles) in water solution as a function of the surface area of nanoparticles. (b) HLS values of the first hyperpolarizability (β') per Pt atom (green disks, this work) and per Au particle[15] (blue triangles) in water solution as a function of the diameter of nanoparticles. The straight lines results from a linear fit with a remarkable correlation coefficient (0.999 for β per Pt particle and 0.999 for β' per Pt atom). The β and β' values from Galletto's work[15] have been recalculated according to the procedure described in the text.

While β values are actually measured per nanoparticle, for comparison between PtNFs of various sizes, it is interesting to study the β' values (hyperpolarizability per Pt atom) which are given by

$$\beta' = \frac{\beta}{\sqrt{N}} \qquad (2)$$

where N is the number of Pt atoms per particle. The β' values per Pt atom have been inferred from β values of PtNFs, as already calculated by other authors[11,14] for other metallic nanoparticles. For this purpose, the volume of PtNFs must be determined.

The β values per particle increase with the surface area of PtNFs (from 2.8 to 61.0×10^{-26} esu), β' increasing with nanoflower diameter (from 260 to 600×10^{-30} esu), in a 7.0 to 31.0 nm diameter range. In Fig. 6a, these results emphasize the strong dependence of the first hyperpolarisability (β) of the platinum colloids on the average surface area of nanoflower. A linear dependence of β per particle with respect to the surface area of PtNFs is observed, indicating a local, dipolar-type response arising from surface effects, as proposed in previous papers.[17]

This linear behavior is similar to that found for the recalculated β and β' values inferred from data by Galletto et al.[15] in AuNSs, using their reported β values per nanoparticle corrected (i) from correct β_{H2O} values (0.055 instead of 0.56×10^{-30} esu)[11] and (ii) using Eq. 2 (see Fig. 6 and Table S1 in the Supporting Information).

The dipolar character of the β values of our PtNFs is confirmed by the polarization-resolved HRS intensity observed for 20nm diameter PtNFs. Upon rotation (0-360 ^{0}) of the incident fundamental polarization, the HLS response is analyzed vertically (Fig. 7a) and horizontally (Fig. 7b). The pattern of the polar plot for a vertical polarization analysis at 2ω corresponds to the expected response of an electric dipole, confirming that the HLS signal from the small metallic nanoparticles is of pure electric dipole origin.

(a)

(b)
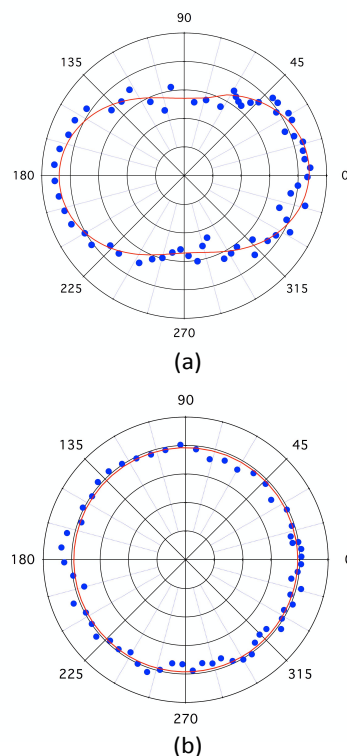
Fig. 7. Polar plot of the input polarization angle dependence of the output-HRS intensity from 20nm diameter PtNFs at 1064nm. (a) Verticality polarized SH scattered light and (b) horizontally polarized SH scattered light.

It has been shown that the first hyperpolarizability of a metal nanoparticle depends on many factors, e.g., the size of the particle, the dielectric constant of the solvent, and particularly the wavelength of the incident light, which is of great importance due to resonance effect. The nature of the metal is also very important and it is interesting to compare β and β' values for NPs with the same diameter and experimental conditions, for different metals. Fig. 6a and 6b demonstrate the higher NLO performances of PtNFs for different surface areas (6a) and particle diameters (6b) as compared to AuNSs. It is interesting to extend this comparison to other noble metal NSs. Here we compare, for particles of the same size (~10, 20 nm), β and β' values of Pt, Au and Ag. For PtNFs, β and β' values are higher than those of Ag and Au NSs. This comparison is presented in Table 3.

Table 3 Comparison between previously observed β values of Ag, Au and Pt NFs (this work) per particle/atom at 1064nm

Metal [Ref.]	Ag[20]	Ag[23]	Au[15]	Au[15]	Pt	Pt
Diameter (nm)	10	20	8.6	22	10	20
Number of atoms per NPs ($\times 10^3$)	32	248	20	330	34	280
β per particle (β) ($\times 10^{-26}$ esu)	1.58	7.0	2.0	16.6	5.7	23.5
β per atom (β') ($\times 10^{-30}$ esu)	90	135	143	291	310	450

We have calculated the HLS intensities expected at 1064nm from the Agarwal-Jha theory[60] applied to Au, Ag and Pt nanospheres, using the optical constants provided by Palik,[61] in order to confirm the prediction made by Johnson et al.[23] at 820 nm. Our calculations confirm Johnson's results at 820 nm, and show that at 1064nm, the ratio of HLS intensities (per atom) between Pt and Au nanospheres is 0.32. Similarly the ratio between Pt and Ag intensities is 0.59. These ratios are higher than those calculated at 820nm, but the superiority of and experimental β values at 1064 nm for PtNFs with respect to those of Ag and Au NS does not fit these calculated results. Most probably the NLO response of PtNFs does not arise mainly from surface plasmon resonance effects, but from specific surface features. In fact, a careful examination of TEM pictures shows that PtNFs are not perfectly spherical, and display a highly corrugated surface. Therefore, the much higher β values reported for PtNFs are induced by surface corrugation with a limited influence of plasmon resonance. This remark is consistent with the results obtained by K. Das et al.[14], this study showing that the β values of low-symmetry, irregularly shaped AuNPs is twice higher than those of centrosymmetric shaped Au nanosphere with a smooth surface. This predominance of corrugation effects seems to be confirmed by the lack of any SHG signal from PtNPs reported in ref.[23,43], these centrosymmetric particles showing smooth

surfaces that did not allow for a significant HLS emission contrary to the present work.

Conclusion

Our work reports the synthesis and characterization of PtNFs with different sizes, controlled by using the seed-mediated method. We have shown for the first time that PtNFs display exceptionally strong first hyperpolarisabilities. These values of PtNFs are found higher than those of gold and silver nanoparticles for particles within the same diameter range. We demonstrated that the first hyperpolarizability (β and β') linearly depends on the surface area and particles diameter of PtNFs, respectively. Particle surface corrugation and shape irregularities seem to be the dominant factor governing these exceptionally high β values. Further studies are currently in progress to gain a better control of PtNPs shape and smoothness in order to provide a more quantitative interpretation of these high nonlinearities.

Materials and methods

Materials

Hexachloroplatinic acid ($H_2PtCl_6.6H_2O$), ascorbic acid ($C_6H_8O_6$) and tri-sodium citrate (TSC, $C_6H_5Na_3O_7.2H_2O$) were purchased from Sigma-Aldrich. The solutions were prepared using ultra-pure water from a Millipore system (18 MΩ cm-1) throughout the experiment. All aqueous samples are at a neutral pH=7.

Synthesis of different shapes of PtNPs

Principle: Pt nanoparticle synthesis is based on the standard reactions.

$$PtCl_6^{2-} + 2C_6H_8O_6 \xrightarrow{100\,^0C} Pt + 6Cl^- + 2C_6H_6O_6 + 4H^+$$

(reduction by ascorbic acid)
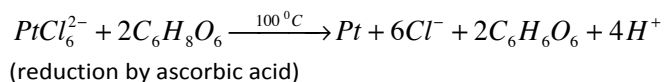
Preparation of 3.0 nm Seed: The first step consists in the preparation of platinum spherical nanoparticle seeds. This preparation was performed starting from a 20 ml aqueous solution of TSC 5×10^{-3} M. Then, 0.2 ml of H_2PtCl_6 0.019 M was added under stirring. After that, 0.1 ml of 0.1 M ascorbic acid was then slowly added and heated to 100 ^{0}C. The colour of solution changed to pale brown. Vigorous stirring of the seed solution was continued for 1 h at 25 ^{0}C before being used. The average particle diameter was 3.0 nm. This solution was then used as the seeding solution for the growth of PtNFs.

Preparation of 7.0; 8.0; 10.0; 14.0 and 20.0 nm PtNFs: In the second step, 20 ml of growth solution, containing 1.9×10^{-4} M H_2PtCl_6 and 5×10^{-3} M TSC, was mixed with 0.1 ml of a 0.1 M freshly prepared ascorbic acid solution. Next, the seed solution of 3.0 nm PtNPs was added and heated to 100^{0}C. Depending on the volume of the added seed solution, the obtained PtNFs show different sizes. With seed solution volumes of 1.0; 0.8; 0.6; 0.4 and 0.2 ml, the resulting solution contained PtNFs with average diameters of 7.0; 8.0; 10.0; 14.0 and 20.0 nm, respectively.

Preparation of 31.0 nm PtNFs: The PtNFs solution containing 7.0 nm diameter particles was used as the seed solution in the third step. 20 ml of the growth solution, containing 1.9×10^{-4} M H_2PtCl_6 and 5×10^{-3} M TSC, was mixed with a 0.1 ml of a 0.1 M freshly prepared ascorbic acid solution. Next, 0.2 ml of the seed solution was added and heated to 100 ^{0}C. The average particle diameter measured from the transmission electron micrograph was 31.0 nm.

Characterization of nanoparticles

The UV-Vis absorption spectrum of the obtained solution was recorded by UV-Vis spectroscopy (Lambda 950) (Fig. 1). XRD spectra of the PtNFs were characterized by using a D8 Advanced Bragg X Ray powder diffraction with Cu Kα radiation at room temperature (Fig. 2). The particles diameters were determined by TEM using a JEOL Model JEM-1400 at 100 kV (Fig. 3).

SHG measurements of PtNFs are performed by HLS at 1.064 μm from a Q- switched Nd^{3+}: YAG nanosecond laser (SAGA from Thales Laser) at a 10 Hz repetition rate. The signal is then detected, sampled, averaged and processed by a computer. A low intensity reference beam is extracted from the main beam at a 45° incidence angle by a glass plate and focused onto a highly nonlinear NPP powder used as a frequency doubler. The variation of the SH intensity scattered from the solution is recorded as a function of the reference SH signal provided by the NPP powder, both signals scaling as the square of the incoming fundamental intensity.

The scattered harmonic signal from a solution is given by:

$$I^{2\omega} = g\left(N_S\left\langle \beta_S^2 \right\rangle + N\left\langle \beta^2 \right\rangle\right)I_\omega^2 \qquad (3)$$

where g is a geometry factor, N_S and N are the number of solvent molecules and nanoparticles per unit volume respectively; β_S and β are the molecular hyperpolarizability of the solvent and nanoparticle, respectively. From the slopes P (respectively P_0) of the lines obtained for the solution (respectively solvent) by recording the variation of $I^{2\omega}$ as a function of $I_{NNP}^{2\omega}$ (the SHG intensity from a reference NLO material (NPP) sample which is proportional to I_ω^2), we can infer the β values of the nanoparticles.[9–11]

Acknowledgements

Notes and references

1 X. Pang, D. He, S. Luo and Q. Cai, *Sens. Actuators B Chem.*, 2009, **137**, 134–138.

2 R. S. Dey and C. R. Raj, *J. Phys. Chem. C*, 2010, **114**, 21427–21433.

3 K. J. Sankaran, S. Kunuku, B. Sundaravel, P.-Y. Hsieh, H.-C. Chen, K.-C. Leou, N.-H. Tai and I.-N. Lin, *Nanoscale*, 2015, **7**, 4377–4385.

4 M.-S. Hu, H.-L. Chen, C.-H. Shen, L.-S. Hong, B.-R. Huang, K.-H. Chen and L.-C. Chen, *Nat Mater*, 2006, **5**, 102–106.

5 W.-C. Law, K.-T. Yong, A. Baev and P. N. Prasad, *ACS Nano*, 2011, **5**, 4858–4864.

6 S. K. Ghosh, M. M. Alam and D. Mandal, *RSC Adv*, 2014, **4**, 41886–41894.

7 X. Ren, X. Meng, D. Chen, F. Tang and J. Jiao, *Biosens. Bioelectron.*, 2005, **21**, 433–437.

8 H. Choi, S.-J. Ko, Y. Choi, P. Joo, T. Kim, B. R. Lee, J.-W. Jung, H. J. Choi, M. Cha, J.-R. Jeong, I.-W. Hwang, M. H. Song, B.-S. Kim and J. Y. Kim, *Nat Photon*, 2013, **7**, 732–738.

9 R. W. Terhune, P. D. Maker and C. M. Savage, *Phys. Rev. Lett.*, 1965, **14**, 681–684.

10 K. Clays and A. Persoons, *Phys. Rev. Lett.*, 1991, **66**, 2980–2983.

11 A. Singh, A. Lehoux, H. Remita, J. Zyss and I. Ledoux-Rak, *J. Phys. Chem. Lett.*, 2013, **4**, 3958–3961.

12 Y. El Harfouch, E. Benichou, F. Bertorelle, I. Russier-Antoine, C. Jonin, N. Lascoux and P.-F. Brevet, *J. Phys. Chem. C*, 2014, **118**, 609–616.

13 C. Hubert, L. Billot, P.-M. Adam, R. Bachelot, P. Royer, J. Grand, D. Gindre, K. D. Dorkenoo and A. Fort, *Appl. Phys. Lett.*, 2007, **90**, 181105.

14 K. Das, A. Uppal, R. K. Saini, G. K. Varshney, P. Mondal and P. K. Gupta, *Spectrochim. Acta. A. Mol. Biomol. Spectrosc.*, 2014, **128**, 398–402.

15 P. Galletto, P. F. Brevet, H. H. Girault, R. Antoine and M. Broyer, *Chem. Commun.*, 1999, 581–582.

16 J. Nappa, G. Revillod, J.-P. Abid, I. Russier-Antoine, C. Jonin, E. Benichou, H. H. Girault and P. F. Brevet, *Faraday Discuss.*, 2004, **125**, 145.

17 I. Russier-Antoine, E. Benichou, G. Bachelier, C. Jonin and P. F. Brevet, *J. Phys. Chem. C*, 2007, **111**, 9044–9048.

18 J. Nappa, G. Revillod, I. Russier-Antoine, E. Benichou, C. Jonin and P. F. Brevet, *Phys. Rev. B*, 2005, **71**, 165407.

19 Y. El Harfouch, E. Benichou, F. Bertorelle, I. Russier-Antoine, C. Jonin, N. Lascoux and P. F. Brevet, *J. Phys. Condens. Matter*, 2012, **24**, 124104.

20 H. M. Ngo and I. Ledoux-Rak, 2014, vol. 9171, p. 91710Y–91710Y–6.

21 P. M. Jais, C. von Bilderling and A. V. Bragas, *Pap. Phys.*, 2011, **3**.

22 C. K. Johnson and S. A. Soper, *J. Phys. Chem.*, 1989, **93**, 7281–7285.

23 R. C. Johnson, J. Li, J. T. Hupp and G. C. Schatz, *Chem. Phys. Lett.*, 2002, **356**, 534–540.

24 E. Shaviv and U. Banin, *ACS Nano*, 2010, **4**, 1529–1538.

25 B. H. San, J. A. Kim, A. Kulkarni, S. H. Moh, S. R. Dugasani, V. K. Subramani, N. D. Thorat, H. H. Lee, S. H. Park, T. Kim and K. K. Kim, *ACS Nano*, 2014, **8**, 12120–12129.

26 J. W. Hong, S. W. Kang, B.-S. Choi, D. Kim, S. B. Lee and S. W. Han, *ACS Nano*, 2012, **6**, 2410–2419.

27 B. Wickman, Y. E. Seidel, Z. Jusys, B. Kasemo and R. J. Behm, *ACS Nano*, 2011, **5**, 2547–2558.

28 W. Yang, Y. Ma, J. Tang and X. Yang, *Colloids Surf. Physicochem. Eng. Asp.*, 2007, **302**, 628–633.

29 R. Venu, T. S. Ramulu, S. Anandakumar, V. S. Rani and C. G. Kim, *Colloids Surf. Physicochem. Eng. Asp.*, 2011, **384**, 733–738.

30 Z. Peng and H. Yang, *Nano Today*, 2009, **4**, 143–164.

31 M. A. Rigsby, W.-P. Zhou, A. Lewera, H. T. Duong, P. S. Bagus, W. Jaegermann, R. Hunger and A. Wieckowski, *J. Phys. Chem. C*, 2008, **112**, 15595–15601.

32 Y. Kang, L. Qi, M. Li, R. E. Diaz, D. Su, R. R. Adzic, E. Stach, J. Li and C. B. Murray, *ACS Nano*, 2012, **6**, 2818–2825.

33 D. Zhai, B. Liu, Y. Shi, L. Pan, Y. Wang, W. Li, R. Zhang and G. Yu, *ACS Nano*, 2013, **7**, 3540–3546.

Nanoscale Accepted Manuscript

34 J. Lu, I. Do, L. T. Drzal, R. M. Worden and I. Lee, *ACS Nano*, 2008, **2**, 1825–1832.

35 J. Kye, M. Shin, B. Lim, J.-W. Jang, I. Oh and S. Hwang, *ACS Nano*, 2013, **7**, 6017–6023.

36 S. Liao, K.-A. Holmes, H. Tsaprailis and V. I. Birss, *J. Am. Chem. Soc.*, 2006, **128**, 3504–3505.

37 N. R. Shiju and V. V. Guliants, *Appl. Catal. Gen.*, 2009, **356**, 1–17.

38 M. Subhramannia and V. K. Pillai, *J. Mater. Chem.*, 2008, **18**, 5858.

39 N. V. Long, M. Ohtaki, M. Uchida, R. Jalem, H. Hirata, N. D. Chien and M. Nogami, *J. Colloid Interface Sci.*, 2011, **359**, 339–350.

40 C. Wang, H. Daimon, Y. Lee, J. Kim and S. Sun, *J. Am. Chem. Soc.*, 2007, **129**, 6974–6975.

41 D. He, S. Mu and M. Pan, *Carbon*, 2011, **49**, 82–88.

42 P. Kundu, C. Nethravathi, P. A. Deshpande, M. Rajamathi, G. Madras and N. Ravishankar, *Chem. Mater.*, 2011, **23**, 2772–2780.

43 null Ahmadi, null Wang, null Green, null Henglein and null El-Sayed, *Science*, 1996, **272**, 1924–1926.

44 Y. Kang, J. B. Pyo, X. Ye, R. E. Diaz, T. R. Gordon, E. A. Stach and C. B. Murray, *ACS Nano*, 2013, **7**, 645–653.

45 L. Wang, C. Hu, Y. Nemoto, Y. Tateyama and Y. Yamauchi, *Cryst. Growth Des.*, 2010, **10**, 3454–3460.

46 M. N. Mankin, V. Mazumder and S. Sun, *Chem. Mater.*, 2011, **23**, 132–136.

47 S. Kundu and H. Liang, *Langmuir*, 2010, **26**, 6720–6727.

48 H. Song, F. Kim, S. Connor, G. A. Somorjai and P. Yang, *J. Phys. Chem. B*, 2005, **109**, 188–193.

49 X. Hu, T. Wang and S. Dong, *J. Nanosci. Nanotechnol.*, 2006, **6**, 2056–2061.

50 W. Yu, W. Tu and H. Liu, *Langmuir*, 1999, **15**, 6–9.

51 K. Miyabayashi, S. Nakamura and M. Miyake, *Cryst. Growth Des.*, 2011, **11**, 4292–4295.

52 N. C. Bigall, T. Härtling, M. Klose, P. Simon, L. M. Eng and A. Eychmüller, *Nano Lett.*, 2008, **8**, 4588–4592.

53 A. Dandapat, A. Mitra, P. K. and G. De, *Nanomater. Nanotechnol.*, 2013, 1.

54 J. Yin, J. Wang, M. Li, C. Jin and T. Zhang, *Chem. Mater.*, 2012, **24**, 2645–2654.

55 N. Goubet, Y. Ding, M. Brust, Z. L. Wang and M.-P. Pileni, *ACS Nano*, 2009, **3**, 3622–3628.

56 T. Jain, F. Westerlund, E. Johnson, K. Moth-Poulsen and T. Bjørnholm, *ACS Nano*, 2009, **3**, 828–834.

57 Y. Wang, D. Wan, S. Xie, X. Xia, C. Z. Huang and Y. Xia, *ACS Nano*, 2013, **7**, 4586–4594.

58 T. Teranishi, M. Hosoe, T. Tanaka and M. Miyake, *J. Phys. Chem. B*, 1999, **103**, 3818–3827.

59 J. Zyss, J. F. Nicoud and M. Coquillay, *J Chem Phys*, 1984, **81**, 4160–4167.

60 G. S. Agarwal and S. S. Jha, *Solid State Commun.*, 1982, **41**, 499–501.

61 E. D. Palik, *Handbook of optical constants of solids*, Academic Press, New York, 1985.